SENSORLESS OPTIMAL CONTROL OF A FIVE-PHASE INDUCTION MOTOR WITH HARMONIC MINIMIZATION

ZAHIR IDER[1], YACINE BOUREK[1], DJAMEL TAIBI[1]

Keywords: Model predictive torque and speed control; Sensorless optimal control; Extended Kalman filter; Five-phase induction machine; Harmonic minimization.

This work presents a sensorless optimal control strategy (model predictive torque and speed control) applied to a five-phase induction machine. Model predictive control (MPC) is used for both torque and flux control, eliminating the need for traditional field-oriented control (FOC) and direct torque control (DTC) techniques. Additionally, model predictive speed control (MPSC) replaces the conventional PI regulator, ensuring fast response and improved dynamic performance. An extended Kalman filter (EKF) is integrated, allowing for accurate estimation of rotor flux, stator currents, and speed. The components of Clarke currents that contribute to harmonic generation are incorporated into the model-predictive torque control (MPTC) optimization criterion. The simulation results from MATLAB Simulink demonstrate the effectiveness of this strategy.

1. INTRODUCTION

In modern industry, asynchronous machines are widely used due to their simple design, low cost, and high reliability, making them a preferred choice for industrial and household applications [1]. However, in high-power three-phase systems, challenges arise, especially in the power converter. Higher power levels increase switching currents in semiconductor devices, leading to faster wear and shorter lifespan [2]. One solution is to increase the supply voltage, but this puts more stress on the insulation and raises the risk of premature system aging [3].

To address these limitations, polyphase induction machines (with more than three phases) offer a practical alternative. They distribute power more efficiently, reducing phase currents without increasing the supply voltage [4,5]. Additionally, they provide better fault tolerance, allowing continued operation even if part of the inverter fails [6]. Another key benefit is the reduction in torque ripple amplitude and an increase in ripple frequency, leading to smoother operation and lower mechanical vibrations [7].

In this context, optimizing control strategies is essential to achieving high energy efficiency and ensuring a fast and accurate dynamic response. Among advanced techniques, model predictive control (MPC) is widely used for its ability to predict system behavior in real-time while directly handling motor constraints [8,10,11]. By using a precise mathematical model, MPC forecasts the motor's future states and calculates optimal control actions. Unlike traditional methods (FOC and DTC), this approach adapts to changing operating conditions, improving control accuracy and overall performance [9,10].

The cascaded predictive control strategy (MPCC and MPC-based speed control (MPSC)) is applied to a three-phase induction machine (IM) [12]. Another MPC is model predictive torque control (MPTC), which directly regulates electromagnetic torque and flux to ensure fast response and minimize torque ripples. Additionally, MPSC optimally adjusts reference torque based on speed errors, improving both transient and steady-state performance. [12–14].

Integrating a Kalman filter, such as the extended Kalman filter (EKF), further enhances control performance by accurately estimating motor states and filtering measurement noise. The combination of MPSC, MPTC, and Kalman-based estimation significantly improves system robustness, ensuring high-performance control in dynamic operating conditions. [12,15,16]. In this context, we have applied them in our work for a five-phase induction machine, considering the Clarke *x-y* current components in the performance criterion of MPTC to reduce the low-frequency harmonics.

Our contributions in this work include the use of MPC for torque and flux control instead of conventional FOC or DTC strategies, as well as the application of MPC for speed control, replacing the traditional PI regulator. Additionally, we integrate the EKF to estimate rotor flux, stator currents, and speed, eliminating the need for sensors. Furthermore, the *x-y* components of Clarke currents, which generate harmonics, are considered in the MPTC optimization criterion to minimize them. Ultimately, this entire approach is applied to a five-phase induction machine rather than a traditional three-phase machine.

2. MODELLING OF THE MACHINE AND THE FIVE-PHASE INVERTER

2.1 MODELING OF A FIVE-PHASE SQUIRREL-CAGE INDUCTION MACHINE IN THE $\alpha\beta xy$ REFERENCE FRAME

A five-phase squirrel-cage induction machine is analyzed using a transformation to the generalized Clarke reference frame. The stator and rotor variables are projected onto α-β-*x-y* axes. The α-β components represent the torque-producing components, while the *x-y* components are auxiliary components that should ideally not contribute to torque generation.

2.1.1 VOLTAGE EQUATIONS

Since a squirrel-cage rotor does not have externally accessible windings, the rotor voltages are zero (i.e., $v_{r\alpha} = v_{r\beta} = v_{rx} = v_{ry} = 0$). The stator voltage equations are given as follows:

Stator:

$$\begin{cases} v_{s\alpha}=R_s i_{s\alpha}+\frac{d\phi_{s\alpha}}{dt}-\omega_s\phi_{s\beta}, \\ v_{s\beta}=R_s i_{s\beta}+\frac{d\phi_{s\beta}}{dt}+\omega_s\phi_{s\alpha}, \\ v_{sx}=R_s i_{sx}+\frac{d\phi_{sx}}{dt}-\omega_s\phi_{sy}, \\ v_{sy}=R_s i_{sy}+\frac{d\phi_{sy}}{dt}+\omega_s\phi_{sx}. \end{cases} \quad (1)$$

Rotor (Squirrel Cage):

$$\begin{cases} 0=R_r i_{r\alpha}+\frac{d\phi_{r\alpha}}{dt}-(\omega_s-\omega_r)\phi_{r\beta}, \\ 0=R_r i_{r\beta}+\frac{d\phi_{r\beta}}{dt}+(\omega_s-\omega_r)\phi_{r\alpha}, \\ 0=R_r i_{rx}+\frac{d\phi_{rx}}{dt}-(\omega_s-\omega_r)\phi_{ry}, \\ 0=R_r i_{ry}+\frac{d\phi_{ry}}{dt}+(\omega_s-\omega_r)\phi_{rx}. \end{cases} \quad (2)$$

[1] Department of Electrical Engineering, Faculty of Applied Sciences, K.M. Ouargla University, 30000, Algeria.
E-mails: ider.zahir@univ-ouargla.dz, bourek.yacine@univ-ouargla.dz, taibi.djamel@univ-ouargla.dz.

2.1.2 FLUX–CURRENTS RELATIONS

The stator and rotor flux linkages are related to the phase currents as follows:

Stator:

$$\begin{cases} \phi_{s\alpha}=L_s i_{s\alpha}+L_m i_{r\alpha}, \\ \phi_{s\beta}=L_s i_{s\beta}+L_m i_{r\beta}, \\ \phi_{sx}=L_s i_{sx}+L_m i_{rx}, \\ \phi_{sy}=L_s i_{sy}+L_m i_{ry}. \end{cases} \qquad (3)$$

Rotor:

$$\begin{cases} \phi_{r\alpha}=L_r i_{r\alpha}+L_m i_{s\alpha}, \\ \phi_{r\beta}=L_r i_{r\beta}+L_m i_{s\beta}, \\ \phi_{rx}=L_r i_{rx}+L_m i_{sx}, \\ \phi_{ry}=L_r i_{ry}+L_m i_{sy}. \end{cases} \qquad (4)$$

2.1.3 ELECTROMAGNETIC TORQUE

For a five-phase induction machine, the electromagnetic torque is given by:

$$T_e=\frac{5}{2}p(\phi_{s\alpha} i_{s\beta}-\phi_{s\beta} i_{s\alpha}). \qquad (5)$$

Since the x-y components ideally do not contribute to torque generation, they are not included in this expression.

2.1.4 MECHANICAL DYNAMICS OF THE ROTOR

The equation describing the mechanical dynamics of the rotor is:

$$J\frac{d\omega_m}{dt}=T_e-T_L-B_m\omega_m. \qquad (6)$$

where:
- J is the rotor inertia,
- T_e is the developed electromagnetic torque,
- T_L is the applied load torque,
- B_m is the viscous friction coefficient.
- ω_m is rotor speed.

2.2 FIVE-PHASE VOLTAGE SOURCE INVERTER

The drive system is illustrated in Fig. 1, where the power converter is a five-phase voltage source inverter (VSI) capable of generating $2^5 = 32$ distinct switching states, consisting of 30 active states and two zero states. Each switching state is defined by the binary vector:

$$[S_a,S_b,S_c,S_d,S_e]^T, \quad \text{where} \quad S_i \in \{0,1\}$$

The logic behind these states is as follows:
S_i=0 : The lower switch is ON, and the upper is OFF.
$S_i = 1$: The upper switch is ON, and the lower is OFF.

$$[S_a,S_b,S_c,S_d,S_e]^T, where S_i \in \{0,1\}$$

The logic behind these states is as follows:
$S_i = 0$: The lower switch is ON, and the upper is OFF.
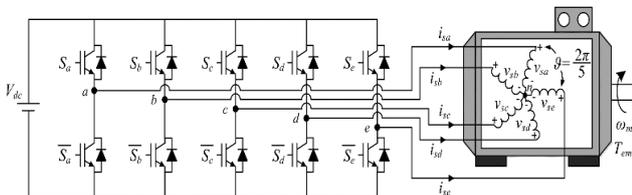$S_i = 1$: The upper switch is ON, and the lower is OFF.

Fig. 1 – Schematic diagram of the five-phase voltage inverter.

Based on this switching configuration, the stator phase voltages V_{si} (where $i = 1,2,3,4,5$) can be determined as a function of the switching states and the DC-link voltage V_{dc} using the following relation [13]:

$$\begin{bmatrix} V_1 \\ V_2 \\ V_3 \\ V_4 \\ V_5 \end{bmatrix}=\frac{V_{dc}}{5}\begin{bmatrix} 4S_1-S_2-S_3-S_4-S_5 \\ 4S_2-S_1-S_3-S_4-S_5 \\ 4S_3-S_1-S_2-S_4-S_5 \\ 4S_4-S_1-S_2-S_3-S_5 \\ 4S_5-S_1-S_2-S_3-S_4 \end{bmatrix} \qquad (7)$$

The Clarke transformation is used to obtain the voltages in the (α, β, x, y) reference frame:

$$\begin{bmatrix} v_{s\alpha} \\ v_{s\beta} \\ v_{sx} \\ v_{sy} \end{bmatrix}=\sqrt{\frac{2}{5}}[M]\begin{bmatrix} V_1 \\ V_2 \\ V_3 \\ V_4 \\ V_5 \end{bmatrix} \qquad (8)$$

where:

$$[M]=\begin{bmatrix} 1 & \cos(\theta_2) & \cos(\theta_3) & \cos(\theta_4) & \cos(\theta_5) \\ 0 & \sin(\theta_2) & \sin(\theta_3) & \sin(\theta_4) & \sin(\theta_5) \\ 1 & \cos(2\theta_2) & \cos(2\theta_3) & \cos(2\theta_4) & \cos(2\theta_5) \\ 0 & \sin(2\theta_2) & \sin(2\theta_3) & \sin(2\theta_4) & \sin(2\theta_5) \end{bmatrix}$$

$$\theta_j=-\frac{2(j-1)\pi}{5}, \quad \text{for } j=2,3,4,5$$

Knowing that, the coordinate transformation is used in the power invariant form, and the zero-sequence component (associated with the z-axis) can be neglected since the windings are star-connected with an isolated neutral point, preventing any zero-sequence current flow [18].

From the two previous eq. (1) and (2), the stator phase voltage components in the α−β and x-y planes are obtained, as illustrated in Fig. 2. Each voltage space vector is represented by an integer corresponding to the digital switching state [Sa Sb Sc Sd Se], [13].
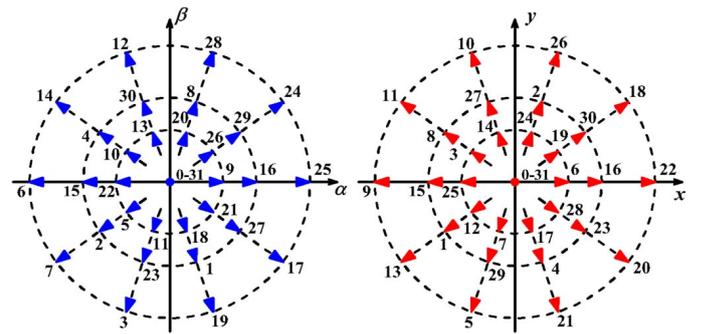

Fig. 2 – Voltage space vectors in the α−β and x−y planes for a two-level five phase inverter [13,17]..

3. MODEL PREDICTIVE TORQUE AND SPEED CONTROL WITH EKF STATES OBSERVER

Figure 3 shows the proposed global structure of a complete speed and torque model predictive sensorless (EKF) control with lower frequency harmonics minimization.

3.1 MODEL PREDICTIVE TORQUE CONTROL EQUATIONS

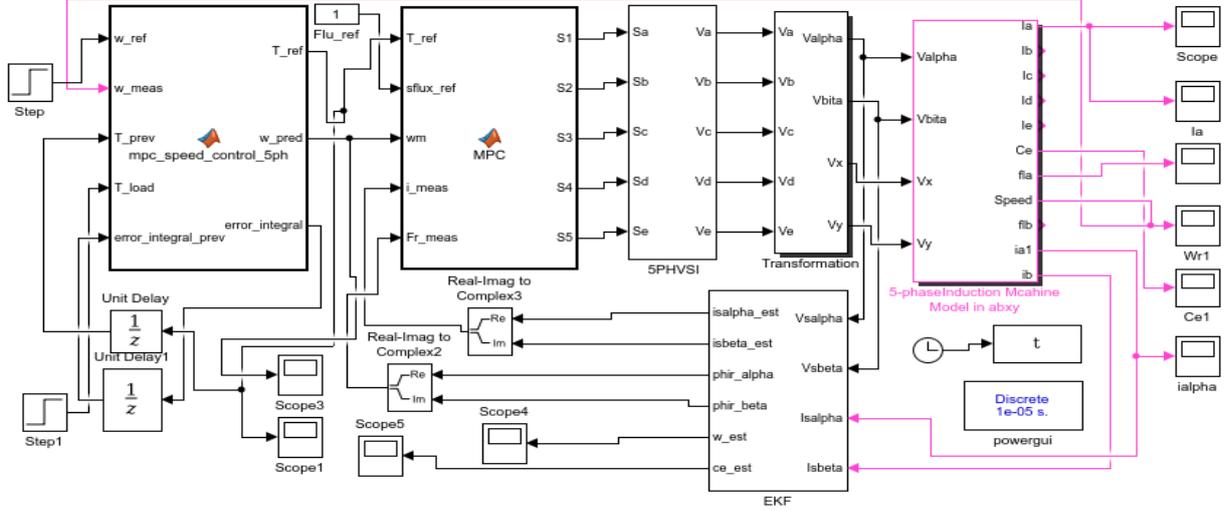The main goal of MPTC is to minimize a cost function to achieve precise torque control while also reducing flux and harmonic distortions, with the consideration of the x-y components of the stator currents in the performance criterion [18].

Fig. 3 — Complete block diagram of 5-phase MPC drive system..

3.1.1 PREDICTION OF STATOR FLUXES

The stator flux estimation from measured rotor flux ϕ_r is given by:

$$\begin{cases} \phi_{s\alpha}^{(k)} = \frac{L_m}{L_r}\left(\phi_{r\alpha}^{meas} - i_\alpha^{meas}\left(L_m - \frac{L_r L_s}{L_m}\right)\right), \\ \phi_{s\beta}^{(k)} = \frac{L_m}{L_r}\left(\phi_{r\beta}^{meas} - i_\beta^{meas}\left(L_m - \frac{L_r L_s}{L_m}\right)\right), \end{cases} \quad (9)$$

$$\begin{cases} \phi_{sx}^{(k)} = \left(L_s - \frac{L_m^2}{L_r}\right)i_{sx}^{meas} + \frac{L_m}{L_r}\phi_{rxy}^{meas}, \\ \phi_{sy}^{(k)} = \left(L_s - \frac{L_m^2}{L_r}\right)i_{sy}^{meas} + \frac{L_m}{L_r}\phi_{rxy}^{meas}. \end{cases} \quad (10)$$

The prediction of stator flux at $(k+1)$:

$$\begin{cases} \phi_{s\alpha}^{(k+1)} = \phi_{s\alpha}^{(k)} + T_s v_{s\alpha} - R_s T_s i_\alpha, \\ \phi_{s\beta}^{(k+1)} = \phi_{s\beta}^{(k)} + T_s v_{s\beta} - R_s T_s i_\beta, \\ \phi_{sx}^{(k+1)} = \phi_{sx}^{(k)} + T_s v_{sx} - R_s T_s i_{sx}, \\ \phi_{sy}^{(k+1)} = \phi_{sy}^{(k)} + T_s v_{sy} - R_s T_s i_{sy}. \end{cases} \quad (11)$$

3.1.2 STATOR CURRENTS PREDICTION

$$\begin{cases} i_{s\alpha}^{(k+1)} = \left(1 + \frac{T_s}{t_\sigma}\right)i_{s\alpha}^{(k)} + \frac{T_s}{t_\sigma + T_s}\left(\frac{1}{r_\sigma}\left(\frac{k_r}{t_r}\phi_{r\alpha}^{meas} - k_r\omega_m\phi_{r\beta}^{meas}\right) + v_{s\alpha}\right), \\ i_{s\beta}^{(k+1)} = \left(1 + \frac{T_s}{\boldsymbol{t_\sigma}}\right)i_{s\beta}^{(k)} + \frac{T_s}{t_\sigma + T_s}\left(\frac{1}{r_\sigma}\left(\frac{k_r}{t_r}\phi_{r\beta}^{meas} + k_r\omega_m\phi_{r\alpha}^{meas}\right) + v_{s\beta}\right), \end{cases} \quad (12)$$

$$\begin{cases} i_{sx}^{(k+1)} = i_{sx}^{(k)} + T_s\left(\frac{1}{L_{xy\sigma}}i_{sx}^{(k)} + \frac{1}{L_{xy\sigma}}\left(v_{sx} - \frac{L_m}{L_r}\phi_{rxy}\right)\right), \\ i_{sy}^{(k+1)} = i_{sy}^{(k)} + T_s\left(\frac{1}{L_{xy\sigma}}i_{sy}^{(k)} + \frac{1}{L_{xy\sigma}}\left(v_{sy} - \frac{L_m}{L_r}\phi_{rxy}\right)\right). \end{cases} \quad (13)$$

3.1.3 PREDIC*T*ION OF ELECTROMAGNETIC TORQUE

$$T_e^{(k+1)} = \frac{5}{2}p\left(\phi_{s\alpha}^{(k+1)}i_{s\beta}^{(k+1)} - \phi_{s\beta}^{(k+1)}i_{s\alpha}^{(k+1)}\right). \quad (14)$$

3.1.4 MINIMIZED COST FUNCTION

$$g = \lambda_c|T_{ref} - T_e^{(k+1)}|^2 + \lambda|\phi_s^* - |\phi_s^{(k+1)}||^2 + \lambda_{\alpha\beta}(|i_{sxy}[k+1]| > i_{sxy\_max}). \quad (15)$$

3.1.5 ALGORITHM OF MODEL PREDICTIVE TORQUE CONTROL (MPTC)

In this algorithm, both the $\alpha\beta$ and xy components are considered to effectively minimize harmonic distortion, leading to improved control performance. The steps of the MPTC algorithm are detailed below:

Step 1: Initialization of Motor Parameters

Compute: $t_r = \frac{L_r}{R_r}$, $\sigma = 1 - \frac{L_m^2}{L_r L_s}$, $k_r = \frac{L_m}{L_r}$,

$r_\sigma = R_s + k_r^2 R_r$, $t_\sigma = \frac{\sigma L_s}{r_\sigma}$,

Define current limits: $i_{xy,max}$.

Step 2: Generation of 32 Switching States i=1 to 32

Extract switching state $(S_1, S_2, S_3, S_4, S_5)$, i=1 to 32

Step 3: Compute phase voltages. Apply Clarke transformation

Step 4: Predict stator fluxes and currents

Step 5: Predict electromagnetic torque

Step 6: Compute cost function

Step 7: Select optimal switching state

$$i^* = \arg\min_i J_i$$

Return $S_1^*, S_2^*, S_3^*, S_4^*, S_5^*$ corresponding to i^*.

3.2 MODEL PREDICTIVE SPEED CONTROL

The classical PI controllers are widely used for speed regulation but suffer from slow response and difficulty handling constraints. The NMC [19], and *sliding mode,* backstepping and fuzzy logic [20,21] the MPC [12], overcomes these issues by predicting system behavior and optimizing control actions in real time. This allows for

faster response, better disturbance rejection, and improved performance compared to traditional PI control.

3.2.1 DYNAMIC MODEL OF ROTOR SPEED

The evolution of the rotor speed is described by eq. (6). By discretizing with a sampling period T_s, we obtain:

$$\omega_r(k+1)=a(k)+bT(k)-\frac{T_L}{J}T_s \tag{16}$$

where

$$a=e^{-\frac{B_m}{J}T_s}, \quad b=\frac{1-A}{B_m}.$$

3.2.2. COST FUNCTION FOR MPC

The goal of the MPC is to minimize the speed error and the torque variation over a prediction horizon N:

$$g_{speed}=\sum_{k=0}^{N-1} Q(\omega_{ref}-\omega_k)^2+RT_k^2, \tag{17}$$

where:

• Q is the weight of the speed error,
• R is the weight of the torque variation.

In matrix form, the cost function can be expressed as:

$$g_{speed}=\frac{1}{2}U^tHU+f^tU, \tag{18}$$

with:

$$H=2(QI_N+RI_N), \quad f=-2Q(\omega_{ref}-X(1)) \tag{19}$$

3.2.3 ANALYTICAL SOLUTIONS FOR CONTROL

The optimal solution is given by:

$$U^*=-H^{-1}f \tag{20}$$

Since H is diagonal, the inversion is straightforward:

$$U^*=-\frac{1}{2(Q+R)}f. \tag{21}$$

The first optimal torque to apply is:

$$T_{ref}=U_1^*+T_L, \tag{22}$$

with saturation:

$$T_{ref}=\min(\max(T_{ref},T_{min}),T_{max}) \tag{23}$$

3.2.4 INTEGRAL ERROR CORRECTION

To improve accuracy, an integral term is added:

$$e(k)=\omega_{ref}-\omega(k), \tag{24}$$

$$e_{int}(k+1)=e_{int}(k)+e(k)T_s, \tag{25}$$

$$g_{speed}=\sum_{k=0}^{N-1} Q(\omega_{ref}+K_ie_{int}-\omega_k)^2+RT_k^2. \tag{26}$$

where: K_i is the integral gain.

3.3 EXTENDED KALMAN FILTER (EKF) EQUATIONS FOR A FIVE-PHASE INDUCTION MACHINE

In MPTC, the EKF-provided state estimates of currents, rotor fluxes, and speed are essential for accurate prediction and optimization. By supplying real-time state information, the EKF enhances control accuracy, disturbance rejection, and overall system performance in MPTC-based control of five-phase induction machines.

3.3.1 STATE-SPACE MODEL

The system is represented as [15]:

$$\begin{cases}\dot{X}=AX+BU+W, \\ Y=CX+V,\end{cases} \tag{27}$$

where:

$x = \begin{bmatrix} i_{s\alpha} & i_{s\beta} & \phi_{r\alpha} & \phi_{r\beta} & \omega_m \end{bmatrix}^t$ is the state vector,
$u = \begin{bmatrix} v_{s\alpha} & v_{s\beta} \end{bmatrix}^t$: the input vector (stator voltages),
$y = \begin{bmatrix} i_{s\alpha} & i_{s\beta} \end{bmatrix}^t$: the measured output vector,
$w\sim N(0,Q)$: the process noise,
$v\sim N(0,R)$: the measurement noise.

3.3.2 MODEL MATRICES

State matrix, control matrix, and observation matrix

$$A=\begin{bmatrix} a_{11} & 0 & a_{13} & a_{14}\omega_m & a_{15}i_{s\beta} \\ 0 & a_{11} & -a_{14}\omega_m & a_{13} & a_{25}i_{s\alpha} \\ a_{31} & 0 & a_{33} & -\omega_m & -\phi_{r\beta} \\ 0 & a_{31} & \omega_m & a_{33} & \phi_{r\alpha} \\ a_{51} & 0 & 0 & 0 & a_{55} \end{bmatrix},$$

$$B=\begin{bmatrix} b_{11} & 0 \\ 0 & b_{11} \\ 0 & 0 \\ 0 & 0 \\ 0 & 0 \end{bmatrix},$$

$$C=\begin{bmatrix} 1 & 0 & 0 & 0 & 0 \\ 0 & 1 & 0 & 0 & 0 \end{bmatrix},$$

where: $T_r=\frac{L_r}{R_r}$, $\sigma=1-\frac{L_m^2}{L_sL_r}$, $a_{11}=-\left(\frac{R_s}{\sigma L_s}+\frac{1-\sigma}{\sigma T_r}\right)$, $a_{13}=\frac{L_m}{\sigma L_s L_r T_r}$, $a_{14}=\frac{L_m}{\sigma L_s L_r}$, $a_{15}=\frac{L_m}{\sigma L_s L_r}$, $a_{25}=-\frac{L_m}{\sigma L_s L_r}$, $a_{31}=\frac{L_m}{T_r}$, $a_{33}=-\frac{1}{T_{aur}}$, $b_{11}=\frac{1}{\sigma L_s}$.

3.3.3 EKF ALGORITHM

The steps of the EKF algorithm are detailed below:

Step 1: Model Discretization

$$\begin{cases} d_F=I+TsA+\frac{(TsA)^2}{2}, \\ G=Ts(I+\frac{Ts}{2}A)B, \end{cases} \tag{28}$$

Step 2: State prediction

$$\hat{x}_{k|k-1}=d_F\hat{x}_{k-1|k-1}+Gu_k, \tag{29}$$

Step 3: Error covariance prediction

$$P_{k|k-1}=d_FP_{k-1|k-1}d_F^T+Q, \tag{30}$$

Step 4: Kalman gain calculation

$$S_k=CP_{k|k-1}C^T+R, \tag{31}$$

$$K_k=P_{k|k-1}C^TS_k^{-1}, \tag{32}$$

Step 5: State update

$$\hat{x}_{k|k}=\hat{x}_{k|k-1}+K_k(y_k-C\hat{x}_{k|k-1}), \tag{33}$$

Step 6: Error covariance update

$$P_{k|k}=(I-K_kC)P_{k|k-1}. \tag{34}$$

4. MATLAB SIMULATION RESULTS

Three simulation tests were performed using MATLAB/Simulink (Fig. 3) over a two-second period, with identical machine parameters, reference values, load torque, and constraints on both currents and torque. The operating scenario features a no-load start, load application at $t = 0.6$ s, and a reversal of rotation at $t = 1$ s. Additionally, low-frequency current harmonics were analyzed on current i_{sa} over 67 cycles at 50 Hz. The three tests are:

– A comparison of MPTC with a conventional PI speed regulator versus an MPSC, as shown in Fig.4.
– An assessment of the complete MPTC scheme with the integration of an EKF for estimating unmeasurable quantities as shown in Fig.5.
– An evaluation of MPTC performance when the i_{xy} current components are incorporated into the cost function, as shown in Table 2.

4.1 SPEED AND TORQUE MODEL PREDICTIVE CONTROL

Figure 4 shows the simulation results of speed and torque MPC in (a), while (b) and (c) present zoomed-in views of speed and torque during the transient regime (startup, load application, and rotation reversal).
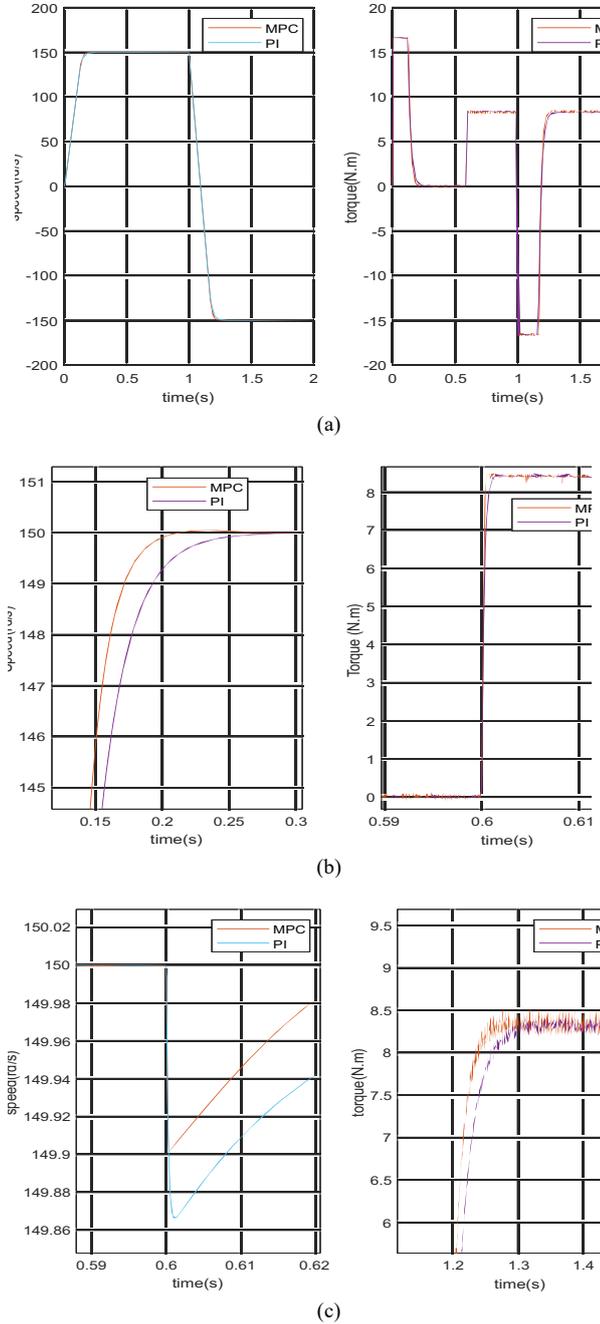

(a)

(b)

(c)

Fig.4 – Simulation results of torque and speed MPC without EKF.

4.2 SPEED AND TORQUE MODEL PREDICTIVE CONTROL WITH EKF

Figure 5 shows the torque and speed results with EKF integration for estimating stator currents and rotor fluxes. The results of Fig. 4 and Fig. 5 show the improvements in torque control, speed tracking, and the rapid recovery of speed after load application. The torque ripple (with EKF estimation) and current low-frequency harmonic reduction.
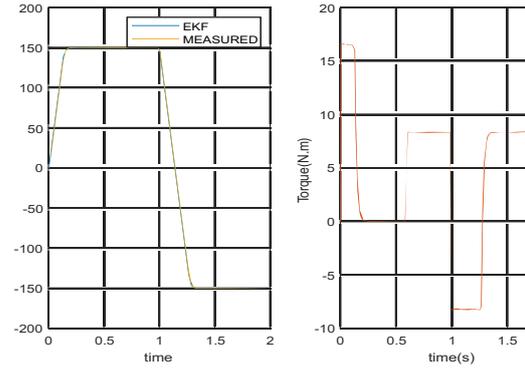

Fig. 5 – Simulation results of torque and speed MPC with EKF/

4.3 COMPARISON OF CONTROL METHODS ON HARMONICS REDUCTION

Table 2 presents the FFT analysis of low-frequency harmonics (as a percentage of the fundamental) of phase current, for three cases: MPC alone, MPC with the inclusion of *x-y* components in the optimization criterion (MPC$_{xy}$), and finally, MPC with EKF integration for estimating stator currents and rotor fluxes. The results show that both strategies, EKF and the consideration of *x-y* components in the minimization criterion of MPTC, help reduce the amplitude of low-frequency harmonics, but the latter (MPC$_{xy}$) is the most effective.

Table 2.

Comparison of low frequency harmonics (% of fundamental)

Method	MPC (%)	MPC$_{xy}$ (%)	MPC+EKF (%)
Harmonic order			
Harmonic H3	45.89	10,19	27.11
Harmonic H5	15.52	3.37	7.75
Harmonic H7	15.16	7.67	7.59
Harmonic H9	20.70	3.44	6.21

5. CONCLUSION

In this work, we use the MPC for torque and flux control instead of conventional FOC or DTC strategies, as well as the application of MPC for speed control, replacing the traditional PI regulator. Additionally, we integrate the EKF to estimate rotor flux, stator currents, and speed, eliminating the need for sensors. Furthermore, the x-y components of Clarke currents, which generate harmonics, are considered in the MPTC optimization criterion to minimize them. Finally, this entire approach is applied to a five-phase induction machine instead of a traditional three-phase machine. The results from these tests highlight improvements in torque control and speed tracking. Torque ripple and current harmonic reduction, demonstrating the effectiveness of the sensorless complete MPC-based approach.

CREDIT AUTHORSHIP CONTRIBUTION STATEMENT

Author_1: Designed the study, developed the simulation models
Author_2: Supervised the work, provided methodological guidance
Author_3: Contributed to the validation of results.

APPENDIX

Table 1

Five-Phase Induction Machine Parameters

Number of Pole Pairs	2
Frequency	50 Hz
Stator Voltage	220 V

Stator Resistance	10 Ω
Rotor Resistance	6.3 Ω
Stator Leakage Inductance	0.46 H
Rotor Leakage Inductance	0.46 H
Magnetizing Inductance	0.42 H
Moment of Inertia	0.0032 kg·m²
Friction Coefficient	0.00114
Nominal speed, ω_m, ω^{meas}, Ω	150 rd/s
Load Torque	8.33 N.m
i_{xy_MAX} constraint	1 A
Torque Min, Max constraint	-16.67, +16.67 N.m
Reference flux	1 Weber

REFERENCES

1. Maafa, H. Mellah, K. Ghedamsi, D. Aouzellag, *Improvement of sliding mode control strategy founded on cascaded doubly fed induction generator powered by a matrix converter*, arXiv preprint arXiv:2208.11140 (2022).

2. R.S. Burye, R.T. Arumalla, S. Figarado, *Investigation of torque ripple in voltage source inverter driven induction motor drive operated with space vector based harmonic elimination pulse width modulation scheme*, arXiv preprint arXiv:2202.01469 (2022).

3. M. Usama, J. Kim, *Vector control algorithm based on different current control switching techniques for AC motor drives*, arXiv preprint arXiv:2005.04651 (2020).

4. R. Krishnan, *Electric motor drives: modeling, analysis, and control*, Prentice Hall, USA (2001).

5. G. Kulandaivel, E. Sundaram, M. Gunasekaran, S. Chenniappan, *Five-phase induction motor drive—a comprehensive review*, Frontiers in Energy Research, **11**, p. 1178169 (2023).

6. E. Levi, *Multiphase electric machines for variable-speed applications*, IEEE Transactions on Industrial Electronics, **55**, *5*, pp. 1893–1909 (2008).

7. M. Jones, E. Levi, *A literature survey of state-of-the-art in multiphase induction motors*, Electric Power Systems Research, **154**, pp. 159–173 (2018).

8. J. Rodriguez, P. Cortes, *Predictive control of power converters and electrical drives*, Wiley-IEEE Press (2012).

9. D.G. Holmes, T.A. Lipo, *Pulse width modulation for power converters: principles and practice*, Wiley-IEEE Press (2003).

10. H. Abu-Rub, M. Malinowski, K. Al-Haddad, *Power electronics for renewable energy systems, transportation and industrial applications*, Wiley (2014).

11. A. Hoggui, A. Benachour, M.C. Madaoui, M.O. Mahmoudi, *Implementation of finite control set model predictive control (FCS-MPC) for five-phase induction motors*, ENP Engineering Science Journal, **5**, *1*, pp. 7–12 (2025).

12. C. Garcia, J. Rodriguez, C. Silva, C. Rojas, P. Zanchetta, H. Abu-Rub, *Full predictive cascaded speed and current control of an induction machine*, IEEE Transactions on Energy Conversion, **31**, *3* (2016).

13. J.A. Riveros, F. Barrero, E. Levi, M.J. Durán, S. Toral, M. Jones, *Variable-speed five-phase induction motor drive based on predictive torque control*, IEEE Transactions on Industrial Electronics, **60**, *8*, pp. 2957–2968 (2013).

14. A. Patidar, D. Sarvate, Y. Nimonkar, *Model predictive torque control of induction motor using SVPWM*, Journal of Management Information and Decision Sciences, **24**, *Special Issue 3*, pp. 1–7 (2021).

15. M.R. Khan, A. Iqbal, *Experimental investigation of five-phase induction motor drive using extended Kalman filter*, Asian Power Electronics Journal, **3** (2009).

16. S. Guedida, B. Tabbache, K. M. S. Benzaoui, K. Nounou, M. Nesri, *Novel speed sensorless DTC design for a five-phase induction motor with an intelligent fractional order controller based on MRAS estimator*, Power Electronics and Drives, **9**, *44*, pp. 63–85 (2024).

17. M. Ahmad, *High performance AC drives: modelling, analysis and control*, Springer (2010).

18. H. Abu-Rub, A. Iqbal, J. Guzinski, *High-performance control of AC drives with MATLAB®/Simulink*, 2nd ed., Wiley, Hoboken, NJ, USA (2021).

19. S.K. Barik, K.K. Jaladi, *Five-phase induction motor DTC-SVM scheme with PI controller and ANN controller*, Procedia Technology, **25**, pp. 816–823 (2016).

20. R. Rouabhi, A. Herizi, S. Djeriou, A. Zemmit, *Hybrid type-1 and 2 fuzzy sliding mode control of the induction motor*, Rev. Roum. Sci. Techn. – Électrotechn. et Énerg., **69**, *2*, pp. 147–152 (2024).

21. A. Herizi, R. Rouabhi, F. Ouagueni, A. Zemmit, *Robust wind power control using sliding mode, backstepping, and fuzzy logic*, Rev. Roum. Sci. Techn. – Électrotechn. et Énerg., **70**, *3*, pp. 313–318 (2025).